Available online at www.sciencedirect.com
SCIENCE DIRECT®
International Journal of Heat and Mass Transfer 47 (2004) 2971–2987
International Journal of HEAT and MASS TRANSFER
www.elsevier.com/locate/ijhmt

Bifurcation and stability of forced convection in curved ducts of square cross-section

Liqiu Wang *, Tianliang Yang

Department of Mechanical Engineering, The University of Hong Kong, Pokfulam Road, Hong Kong

Received 7 November 2003; received in revised form 6 March 2004

Abstract

A numerical study is made on the fully developed bifurcation structure and stability of the forced convection in a curved duct of square cross-section (Dean problem). In addition to the extension of three known solution branches to the high Dean number region, three new asymmetric solution branches are found from three symmetry-breaking bifurcation points on the isolated symmetric branch. The flows on these new branches are either an asymmetric two-cell state or an asymmetric seven-cell structure. The linear stability of multiple solutions are *conclusively* determined by solving the eigenvalue system for all eigenvalues. Only two-cell flows on the primary symmetric branch and on the part of isolated symmetric branch are linearly stable. The symmetric six-cell flow is also linearly unstable to asymmetric disturbances although it was ascertained to be stable to symmetric disturbances in the literature. The linear stability is observed to change along some solution branch even without passing any bifurcation or limit points. Furthermore, dynamic responses of the multiple solutions to finite random disturbances are also examined by the direct transient computation. It is found that possible physically realizable fully developed flows evolve, as the Dean number increases, from a stable steady two-cell state at lower Dean number to a temporal periodic oscillation state, another stable steady two-cell state, a temporal intermittent oscillation, and a chaotic temporal oscillation. Among them, three temporal oscillation states have not been reported in the literature. A temporal periodic oscillation between symmetric/asymmetric two-cell flows and symmetric/asymmetric four-cell flows are found in the range where there are no stable steady fully developed solutions. The symmetry-breaking point on the primary solution branch is determined to be a subcritical Hopf point by the transient computation.

1. Introduction

As the first part of the work on the multiplicity and stability of combined free and forced convection in rotating curved ducts, the present contribution addresses the fully developed bifurcation structure and stability of the forced convection in a stationary curved duct of square cross-section (Dean problem) [1]. The flow geometry is illustrated in Fig. 1 with (R, Z, ϕ) as the radial, spanwise and streamwise directions, respectively. A viscous fluid is driven by a streamwise pressure gradient to flow through a square duct with a streamwise curvature and an uniform wall heat flux. Such flows and transport phenomena have been, and still are, the object of intense investigations, due to its intrinsic interest, as well as its relevance to a host of areas involving curved passages and surfaces. The readers are referred to [2–5] for some comprehensive and outstanding reviews of the Dean problem. For our purposes, we focus our brief literature review mainly on flow bifurcation and stability of fully developed solutions in curved ducts of square cross-section with increasing Dean numbers. The Dean number De is the dynamical parameter of the problem and is defined by $De = Re\sqrt{\sigma}$. Here Re is the Reynolds number. σ is the curvature ratio defined by a/R_c, the ratio of duct width a over the radius of curvature R_c (Fig. 1).

* Corresponding author. Tel.: +852-2859-7908; fax: +852-2858-5415.
E-mail address: lqwang@hkucc.hku.hk (L. Wang).

0017-9310/$ - see front matter © 2004 Elsevier Ltd. All rights reserved.
doi:10.1016/j.ijheatmasstransfer.2004.03.002

Nomenclature

a	duct width
c_1	streamwise pressure gradient
c_2	streamwise temperature gradient
De	Dean number; $Re\sqrt{\sigma}$
Dk	pseudo-Dean number
p	dimensionless pseudo-pressure
P	pseudo-pressure
Pr	Prandtl number
r, z	dimensionless coordinates; $r = R/a$, $z = Z/a$
R, Z, ϕ	coordinates
R_c	curvature radius
Re	Reynolds number; $W_m a/v$
t	time
T	fluid temperature
T_w	wall temperature
u, v, w	dimensionless velocity components
U, V, W	velocity components in directions of R, Z and ϕ, respectively
W_1	representative streamwise velocity
W_m	streamwise mean velocity

Greek symbols

α	fluid thermal diffusivity
μ	fluid dynamic viscosity
v	fluid kinematic viscosity
ψ	stream function
ρ	fluid density
σ	curvature ratio; a/R_c
τ	dimensionless time
θ	dimensionless temperature
ΔT	representative temperature difference

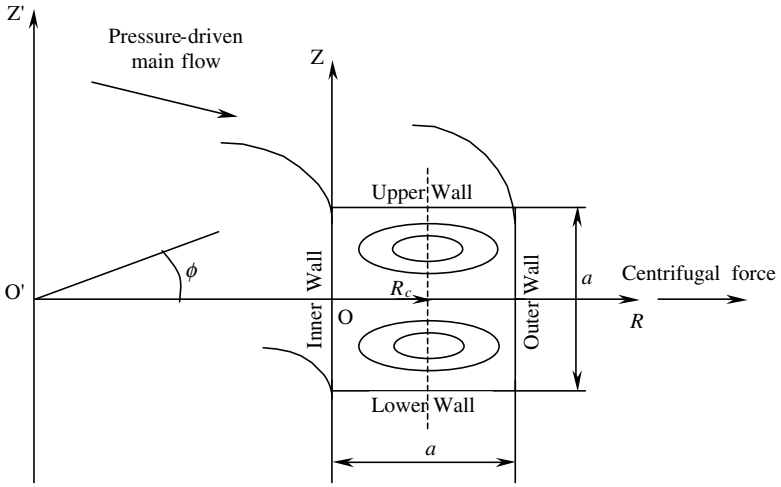

Fig. 1. Physical problem and coordinate system.

Existence of upper and lower walls induces pressure gradients along the walls, which manifest themselves as one pair of counter-rotating vortices on the cross plane [6,7]. These vortices are called the Ekman vortices in literature and are present for any non-zero value of Dean number. As a consequence, the fully developed flow in a curved square duct is a symmetric two-cell state at lower Dean numbers. As the Dean number increases, this two-cell flow loses its stability due to a centrifugal instability (also called Dean instability in literature) [8]. As explained in [9], in the region near the central outer wall, the pressure gradient across the duct in the radial direction is positive but the centrifugal force decreases from a maximum value to zero at the outer wall. The instability due to the imbalance between the inward pressure gradient and the outward centrifugal force generates an unstable region. Cheng and Akiyama [10] first reported, by their numerical study of loosely coiled ducts of rectangular cross-section, that this instability manifests itself in form of a secondary pair of counter-rotating vortices near the central outer wall. The fully developed flow in a square duct is thus a four-cell state in which the secondary pair of vortices near the central outer wall are named as the Dean vortices. This four-cell flow was further detailed numerically in [9,11,12], and was confirmed experimentally in [13,14]. The critical Dean number for the switch from the two-cell pattern to the four-cell pattern was found to be about 118 in [9,13],

while it was reported to be about 100 for square ducts in [12]. The difference regarding this critical value indicates the existence of a range of Dean numbers where two- and four-cell solutions co-exist.

Such co-existence of two- and four-cell solutions was described in [15]. Masliyah [16] established this co-existence both numerically and experimentally for the fully developed flow in a curved duct of semicircular cross-section with a flat outer wall. Numerical studies in [17–20] also found dual solutions for fully developed flow in a curved duct of square cross-section.

Detailed bifurcation structure and linear stability of solutions for steady fully developed flows in a curved duct of square cross-section was determined numerically by Winters [19]. Three solution branches were found. For a loosely coiled duct with $\sigma = 0.04$, the primary branch starts at low Dean number as a symmetric (w.r.t. the horizontal central plane) two-cell flow state (two large counter-rotating Ekman vortices), and develops as increasing Dean number to a symmetric four-cell flow (two large Ekman vortices and two small Dean vortices near the center of the outer wall) through two limit points at $De = 131$ and $De = 113$. Between these two limit points, two-cell and four-cell solutions co-exist. The linear stability analysis in [19] determined that the two-cell flow is stable and the four-cell flow is unstable with respect to asymmetric disturbances. Bara et al. [21] experimentally confirmed, using a curved duct of 270° and constant curvature ratio of 0.0662, the solution structure up to $De = 150$, including the dual solution region. They observed the symmetric flow although it is unstable because the asymmetric disturbances in their apparatus were small or the flow had not reached the fully developed state in their 270° curved duct.

The second branch found in [19] is a pair of asymmetric solutions. This branch has two pairs of limit points and arises from a symmetry-breaking bifurcation point at $De = 130$ on the primary branch. The flow, consisting of two asymmetric Ekman vortices, is unstable. The third branch is an isolated branch of two-cell and four-cell flows above $De = 191$. Winters [19] determined that the isolated symmetric four-cell sub-branch is unstable while the isolated two-cell sub-branch is stable. The location of limit and bifurcation points does not change much for curvature ratios less than 0.2, but at higher curvature ratios (tighter coil), they move to higher Dean numbers.

Therefore, no stable steady fully developed solutions exist between $De = 131$ and $De = 191$. This raises the question of what are the physically realizable solutions in this region. Clearly, the flows must develop steady spatial (streamwise) oscillations or fully developed temporal oscillations, or even some combination of the two. Experimentally, both oscillations were observed between symmetric/asymmetric two-cell flows and symmetric/asymmetric four-cell flows for Dean number up to 269 [21–27]. The co-existence of both kinds of oscillations could be the result of development of different disturbances in the experimental apparatus. Sankar et al. [28] predicted steady spatial oscillations at Dean number above 128 numerically by using a parabolized version of steady, three-dimensional Navier–Stokes equations. However, there is no known study on prediction of fully developed temporal oscillations and how such oscillations relate to the solution structure outlined above. This partly motivates the present study to predict the temporal oscillations and find their relation with the solution structure.

It is noted that the upper limit of oscillating flow region is higher than predicted in [19] (at $De = 191$). This leads to the question of whether the isolated two-cell branch is stable near the limit point of $De = 191$. The stability indicator used in [19] was the sign of Jacobian determinant which equals $(-1)^n$, where n is the number of negative eigenvalues of the Jacobian matrix. A negative value of this indicator indicates instability, but a positive value is *insufficient* to indicate stability [19]. Therefore, the linear stability of solutions with a positive Jacobian determinant, including the isolated two-cell branch, has not been conclusively determined. Furthermore, the *branch* stability is often determined by the stability of one point on the branch. This is partly due to the fact that the computation of the complete eigenvalue spectrum along solution branches is a computationally expensive process and partly due to the assumption prevalent in the literature that the linear stability of solutions along a solution branch is unchanged without passing limit/bifurcation points. However, based on the bifurcation and stability theory, such a change in stability is possible [29]. Therefore, a more detailed and careful linear stability analysis is desirable to *conclusively* determine the linear stability of multiple solutions. This also partly stimulates the present study.

Daskopoulos and Lenhoff [20] extended the work by Winters [19] to a higher Dean number. While no new solution branches were detected, four limit points on the isolated two-cell branch were found as the Dean number increased. Some of these points lead to solutions with six or eight vortices. Note that Daskopoulos and Lenhoff [20] have imposed a symmetry condition on the horizontal central plane. Thus questions concerning asymmetric solutions, their stability and symmetry-breaking bifurcations have been left unanswered. This forms another motivation behind the present study.

While the linear stability analysis is efficient in terms of the computation efforts required, it suffers two fundamental defects. First, it is not applicable to a finite disturbance. With a finite disturbance, a stable solution based on the linear stability may not be always stable. Second, it provides no answer to questions related to the dynamic behavior of the solutions, including how flows approach a stable solution after a disturbance, what

happens to an unstable solution after a disturbance, whether all unstable solutions at a given set of parameters respond disturbances in the same way, and whether the disturbances lead an unstable solution to the stable one at the same parameter value. Clearly, a fully transient computation is necessary to examine dynamic responses of the multiple solutions to finite random disturbances. This forms another motivation behind the present work.

The bifurcation and stability of the multiple solutions available in literature are limited to low Dean numbers (less than 250). However, solutions and their stability at high Dean numbers are more relevant for practical applications. Upon increasing the Dean number, a richer bifurcation structure and a more intricate stability feature are expected because of a stronger nonlinearity of the problem. New limit/bifurcation points and solution branches are expected. Because of the lack of the solution structure at high Dean numbers, there is a long-standing controversy over such solutions obtained by different methods that aimed at obtaining a solution without considering the multiplicity. To resolve this controversy, we need to find the bifurcation structure at high Dean numbers. Furthermore, it is also reasonable on the physical ground to expect phenomena related to the transition to the turbulence at high Dean numbers such as oscillation solutions, periodic doubling, intermittency, and chaotic oscillation. This also stimulates the present work to extend the previous works to a range with higher Dean numbers and to examine dynamic responses of the multiple solutions to finite random disturbances by the direct transient computation.

The present work is a relatively comprehensive study on the bifurcation structure and stability of multiple solutions for the laminar forced convection in a curved duct of square cross-section (Fig. 1). The governing differential equations in primitive variables and in stream function and vorticity are solved for detailed bifurcation structure by a finite-volume/Euler–Newton continuation method with the help of the bifurcation test function, the branch switching technique and the parameterization of arc-length or local variable. Transient calculation is made to examine in detail the response of every solution family to finite random disturbances. Eigenvalue systems are solved for all eigenvalues by QR decomposition method to conclusively determine the linear stability of the multiple solutions. The Hopf bifurcation can also be detected by the transient computation and by the appearance of a pair of pure imaginary conjugated eigenvalues in the linear stability analysis. The power spectra are constructed by the Fourier transformation of temporal oscillation solutions to confirm the chaotic flow at large Dean numbers. We restrict ourself to the hydrodynamically and thermally fully developed region and two-dimensional disturbances. So far, a detailed 3D numerical computation of flow bifurcation and stability is still too costly to conduct. A 2D model is still useful for a fundamental understanding of curved duct flows. However, our assumption of fully developed flow limits our analysis to the one preserving the streamwise symmetry. There may be further bifurcation to flows that breaks this symmetry and that cannot be found in the present work.

In addition to the three solution branches in [19,20], three new asymmetric branches are found from three symmetry-breaking bifurcation points on the isolated symmetric branch. Only symmetric two-cell flows on the primary branch and on some part of isolated two-cell branch are linearly stable. The linear stability of the isolated two-cell branch changes along the branch. In the range where there is no stable steady fully developed solution, flows develop into a temporal periodic oscillation state between symmetric/asymmetric two-cell flows and symmetric/asymmetric four-cell flows. As the Dean number increases in the region studied in present work, possible physically realizable fully developed flows evolute from a stable steady two-cell state at lower Dean number to a temporal periodic oscillation state, another stable steady two-cell state, an intermittent oscillation, and a chaotic state. Among them, three temporal oscillation states have not been reported in the literature. Furthermore, the intermittency is found to lead curved duct flows to chaos. The temporal periodic oscillation serves as, on the other hand, the transition from one stable steady flow to another.

2. Governing parameters and numerical algorithm

Consideration is given to a hydrodynamically and thermally fully developed laminar flow of viscous fluid in a curved square duct under the thermal boundary conditions of uniform wall heat flux and peripherally uniform wall temperature at any streamwise position (Fig. 1). The geometry is toroidal and hence the finite pitch effect is not considered. Properties of the fluid, the density in particular, are taken to be constant. Therefore, a gravity potential can be introduced for the purely hydrostatic effect of gravity.

Consider an toroidal coordinate system (R, Z, ϕ) as shown in Fig. 1. Let U, V and W be velocity components in directions of R, Z and ϕ respectively, t the time, and T, T_w the temperature of the fluid and the wall. Continuity, Navier–Stokes and energy equations governing the fully developed laminar flow and heat transfer are given, in terms of dimensionless variables, as [10,30,31]:

Continuity equation

$$\frac{\partial}{\partial r}\{[1+\sigma(r-0.5)]u\}+\frac{\partial}{\partial z}\{[1+\sigma(r-0.5)]v\}=0. \quad (1)$$

Momentum equations

$$\frac{\partial u}{\partial \tau}+u\frac{\partial u}{\partial r}+v\frac{\partial u}{\partial z}-\frac{16w^2Dk^2}{\sigma[1+\sigma(r-0.5)]} = -\frac{\partial p}{\partial r}+\left\{\frac{\partial^2 u}{\partial r^2}+\frac{\partial^2 u}{\partial z^2}+\frac{\sigma}{1+\sigma(r-0.5)}\frac{\partial u}{\partial r} -\frac{\sigma^2 u}{[1+\sigma(r-0.5)]^2}\right\}, \tag{2}$$

$$\frac{\partial v}{\partial \tau}+u\frac{\partial v}{\partial r}+v\frac{\partial v}{\partial z}=-\frac{\partial p}{\partial z}+\left[\frac{\partial^2 v}{\partial r^2}+\frac{\partial^2 v}{\partial z^2}+\frac{\sigma}{1+\sigma(r-0.5)}\frac{\partial v}{\partial r}\right], \tag{3}$$

$$\frac{\partial w}{\partial \tau}+u\frac{\partial w}{\partial r}+v\frac{\partial w}{\partial z}+\frac{\sigma uw}{1+\sigma(r-0.5)} = \frac{1}{1+\sigma(r-0.5)}+\left\{\frac{\partial^2 w}{\partial r^2}+\frac{\partial^2 w}{\partial z^2}+\frac{\sigma}{1+\sigma(r-0.5)}\frac{\partial w}{\partial r} -\frac{\sigma^2 w}{[1+\sigma(r-0.5)]^2}\right\}. \tag{4}$$

Energy equation

$$\frac{\partial \theta}{\partial \tau}+u\frac{\partial \theta}{\partial r}+v\frac{\partial \theta}{\partial z}-\frac{4wDk}{\sigma Pr[1+\sigma(r-0.5)]} = \frac{1}{Pr}\left[\frac{\partial^2 \theta}{\partial r^2}+\frac{\partial^2 \theta}{\partial z^2}+\frac{\sigma}{1+\sigma(r-0.5)}\frac{\partial \theta}{\partial r}\right]. \tag{5}$$

The dimensionless variables are defined as:

$$r=\frac{R}{a},\quad z=\frac{Z}{a},\quad \tau=\frac{t}{v/a^2},$$

$$u=\frac{aU}{v},\quad v=\frac{aV}{v},\quad w=\frac{W}{W_1},$$

$$p=\frac{P}{\rho(v/a)^2},\quad \theta=\frac{T_w-T}{\Delta T},$$

where v and ρ are the kinematic viscosity and the density of the fluid, a is the duct radial dimension, P is a pseudo-pressure, a combination of fluid pressure and the gravity potential, W_1 and ΔT are the representative streamwise velocity and temperature difference, respectively, which are defined as

$$W_1=\frac{a^2c_1}{\mu};\quad \Delta T=Pr\,ac_2.$$

Here μ is the viscosity of the fluid, Pr the Prandtl number, c_1 the streamwise pressure gradient which is a positive constant for hydrodynamically fully developed flow ($c_1=-\frac{\partial P}{R_c\partial\phi}$ with R_c as the curvature radius, [30]), c_2 the streamwise temperature gradient which is a constant for the thermally fully developed flow, but can be positive or negative depending on heating or cooling of the fluid ($c_2=\frac{\partial T}{R_c\partial\phi}$, [30,32,33]).

Three dimensionless parameters are defined as:

$$\sigma=\frac{a}{R_c},\quad Pr=\frac{v}{\alpha},\quad Dk=\frac{\sigma aW_1}{4v},$$

with α as the thermal diffusivity. The dimensionless groups adopted here are those in [30,31]. The curvature ratio σ is a geometry parameter, representing the degree of curvature. The Prandtl number Pr, a thermophysical property parameter, represents the ratio of momentum diffusion rate to that of thermal diffusion. Dk is a pseudo-Dean number with W_1 as the characteristic velocity, representing the ratio of the square root of the product of inertial and centrifugal forces to the viscous force [30,31]. It characterizes the effect of inertial and centrifugal forces. Among the three parameters, the curvature ratio σ is a more detailed measure of the effect of geometry and the extent to which the centrifugal force varies on the cross-section. Winters [19] found that it does not contribute to the structural change of bifurcation while higher curvature ratios (larger than 0.2) shift limit and bifurcation points to higher Dean numbers. This is consistent with the Dean's theoretical finding that the Dean problem is governed by the Dean number alone for the loosely coiled ducts [2,5]. Therefore, we fix its value at 0.02, typically used in cooling systems of rotor drums and conductors of electrical generators. While the Prandtl number Pr affects the temperature field, it has no effect on flows because the flow field is decoupled with the temperature field for the forced convection. In the present work, we set the Pr at 0.7, a typical value for air.

Boundary conditions (non-slip, impermeability and uniform peripheral temperature) may be written, in terms of dimensionless variables, as

$$u=v=w=\theta=0 \quad \text{at } r=0,1 \quad \text{for } -0.5\leqslant z\leqslant 0.5 \tag{6}$$

$$u=v=w=\theta=0 \quad \text{at } z=-0.5,0.5 \quad \text{for } 0\leqslant r\leqslant 1 \tag{7}$$

The formulation of the problem is on full flow domain without imposing symmetric boundary conditions to perform a thorough numerical simulation.

The details of numerical algorithms are available in [34]. For steady bifurcation structure, the governing differential equations without the time-dependent terms are discretized by the finite volume method to obtain discretization equations. The method is an adaptation of that in [31,35]. Its main features include a staggered mesh system, a power-law formulation for the combined effect of convection and diffusion terms, and central difference scheme for source terms.

The discretization equations are solved for parameter-dependence of velocity, pressure and temperature fields by the Euler–Newton continuation method [29,36].

The solution branches are parameterized by Dk for the regular portion of the branch, the arc-length or the dimensionless radial velocity component u at $r = 0.9$ and $z = 0.14$ for turning limit points [29,36]. Here $r = R/a$, $z = Z/a$ (Fig. 1). The u at (0.9, 0.14) is selected as the control parameter in turning limit points because it varies significantly with Dk. The starting point of our continuation algorithms is that of $Dk = 0$. The bifurcation points are detected by the test function in [29]. The branch switching is made by a scheme approximating the difference between branches proposed in [29]. The linear stability and the dynamic response of multiple steady solutions to the 2D finite random disturbances are examined by the QR decomposition method and the direct transient computation, respectively. The random disturbance is generated by $d^{(k)}\chi^{(k)}\mathbf{y}_s$. Here d is the maximum percentage of disturbing value over the steady value $\mathbf{y}_s$. The superscript k represents the ordinal of the disturbance. χ is a vector whose components take random values from -1 to 1 and are generated by the computer. The readers are referred to [34] for the numerical details.

With the recognition that at a point in the parameter space, several different solutions with quite different flow structures can co-exist, a uniform grid that is fine enough to resolve all the different flow structures appears proper. A careful study of the grid dependence by using different grid sizes shows that 50×50 is a reasonably accurate choice for the grid size [34]. To verify the code, five representative properties obtained by the present work is shown in Table 1 together with those in [31] at $Dk = 100$, $\sigma = 0.02$ and $Pr = 0.7$, where there is only one solution. They are Reynolds number defined by $Re = W_m a/\nu$ with W_m as the streamwise mean velocity, Dean number ($De = Re\sqrt{\sigma}$), maximum of absolute values of secondary flow stream function ($|\psi|_{max}$), maximum streamwise velocity (w_{max}) and maximum temperature (θ_{max}). The results are in good agreement, with a very small difference (less than 2%) being due to the different numerical methods used in two studies. We also compared, in Table 2, the locations (in terms of their De values) of three limit points S_1^1, S_1^2, S_2^1 and one bifurcation point B_1 with those available in [19] (see next section for the notation of limit points). The results of the present analysis are also in good agreement with those in [19]. The very small difference (less than 1.5%) is believed to be due to the different numerical methods used in two studies.

Table 1
Comparison of five representative properties at $Dk = 100$, $\sigma = 0.02$, $Pr = 0.7$ with those in [31]

Sources	Re	De	$\lvert\psi\rvert_{max}$	w_{max}	θ_{max}
Present work	541	76.5	5.528	0.0494	39.7
[31]	542	76.6	5.641	0.0496	39.9

Table 2
Locations of S_1^1, S_1^2, S_2^1 and B_1: a comparison with those in [19]

	S_1^1	S_1^2	S_2^1	B_1
Present work	129.55	112.82	187.91	128.22
[19]	131.13	113.35	190.77	129.71

To further verify the code and accuracy, we re-obtained the bifurcation structure by using a stream function/vorticity version of governing equation and 50×50 uniform grid. The bifurcation structure by these two methods were found to be in excellent agreement in most of range ($Dk \leqslant 700$), and have very slightly quantitative difference when $Dk > 700$ [34].

3. Results and discussion

3.1. Solution structure

The bifurcation structure is shown in Fig. 2 for Dk values from 0 up to 800 at $\sigma = 0.02$ and $Pr = 0.7$. In Fig. 2, the u velocity at (0.9, 0.14) is used as the state variable, enabling the most clear visualization of all solution branches. Six solution branches, labeled by S_1, S_2, A_1, A_2, A_3 and A_4 respectively, are found. Here, S stands for symmetric solutions with respect to the horizontal central plane $z = 0$ and A for asymmetric solutions. Branch A_1 is bifurcated from S_1 at the symmetry-breaking bifurcation point B_1. Branches A_2, A_3 and A_4 are bifurcated from S_2 at three symmetry-breaking bifurcation points B_2, B_3 and B_4, respectively. Table 3 lists Dk and De values of four symmetry-breaking bifurcation points B_1–B_4 and 15 limit points labeled by their branch symbol with a superscript number. For example, S_1^2 represents the second limit point on the solution branch S_1. To visualize the details of branch connectivity and some limit points, the locally enlarged state diagrams are also shown in Fig. 2. As Fig. 2 is only 1D projection of N-dimensional solution branches, all intersecting points except four bifurcation points should not be interpreted as connection points of branches. In terms of Dk, the work in [19] is limited to the range up to about 400. It is interesting to note that there are always odd number of co-existing steady solutions at each Dk from 0 to 800. Note also that each pair of singular points (B_1, A_1^1), (B_2, A_2^1), (B_3, A_3^1) and (B_4, A_4^1) are very close. Two singular points in each pair get closer as the mesh size decreases. Their slight separation is thus an artifact of the numerical discretization.

Among six solution branches, S_1, S_2 and A_1 have been first reported in [19]. We here reconfirm and extend their findings up to $Dk = 800$. While no new limit and bifur-

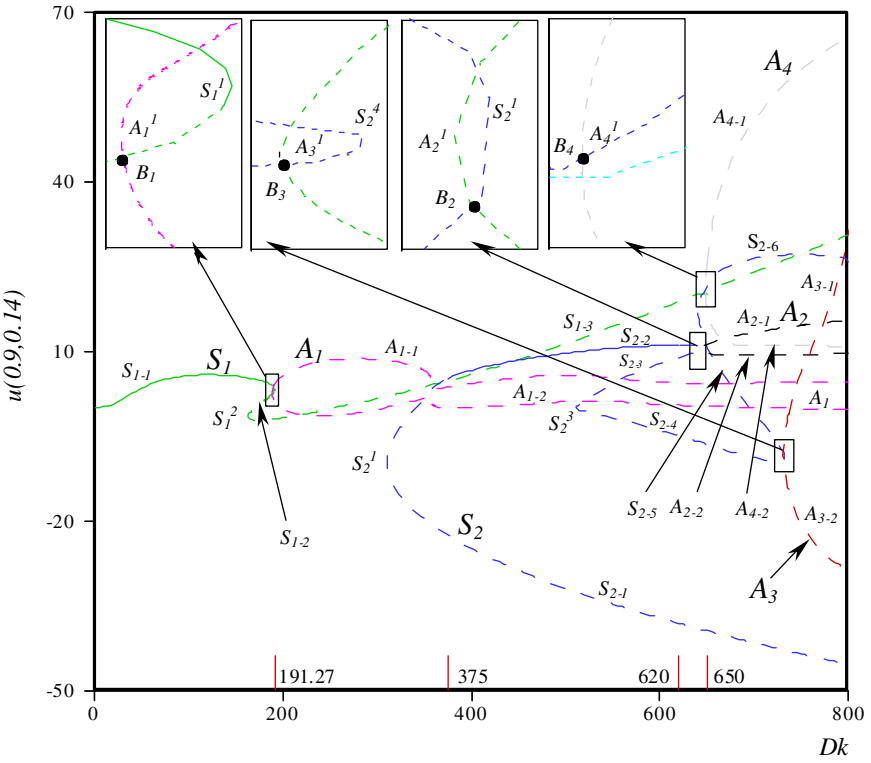

Fig. 2. Solution branches and their connectivity ($\sigma = 0.02$, $Pr = 0.7$).

Table 3
Locations of all limit points and bifurcation points up to $Dk = 800$ at $\sigma = 0.02$ and $Pr = 0.7$

Points	Dk	De
S_1^1	191.27	129.55
S_1^2	163.43	112.82
A_1^1	188.67	127.51
A_1^2	357.41	209.92
A_1^3	355.72	209.25
A_1^4	357.41	209.92
A_1^5	355.72	209.25
S_2^1	310.71	187.91
S_2^2	643.30	325.83
S_2^3	511.04	274.80
S_2^4	732.43	350.41
S_2^5	640.59	319.34
A_2^1	641.87	324.89
A_3^1	730.83	349.84
A_4^1	648.16	322.27
B_1	188.80	128.22
B_2	642.51	325.14
B_3	731.22	350.01
B_4	648.18	322.27

cation points are found along S_1 and A_1, four additional limit points S_2^2–S_2^5 (first reported in [20]) and three new symmetry-breaking bifurcation points B_2, B_3 and B_4 are detected along S_2. In particular three symmetry-breaking bifurcation points B_2, B_3 and B_4 lead to three pairs of asymmetric solution branches A_2, A_3 and A_4.

The primary branch S_1 is a symmetric solution branch. It has two limit points S_1^1 and S_1^2. The two limit points divide the branch into three parts $S_{1\text{-}1}$, $S_{1\text{-}2}$ and $S_{1\text{-}3}$, and generate a range ($163.43 < Dk < 191.27$) where three steady solutions co-exist for a fixed value of Dk. The secondary flows for these three sub-branches are the two-cell state (two Ekman vortices, Fig. 3(a)), the weak four-cell state with two Ekman vortices and two weak Dean vortices (Fig. 3(b)), and the four-cell state with two Ekman vortices and two Dean vortices (Fig. 3(c)), respectively. In the figure, the stream function is normalized by its maximum absolute values $|\psi|_{\max}$. A vortex with a positive (negative) value of the secondary flow stream function indicates a counter-clockwise (clockwise) circulation. The readers are referred to [31] for a detailed discussion of two-cell and four-cell flow structures in general, their relations with physical mechanisms and driving forces and their effects on the flow resistance and heat transfer in particular.

In addition to the two limit points S_1^1 and S_1^2, the primary branch S_1 also has a symmetry-breaking bifurcation point B_1 at $Dk \doteq 188.8$ ($De \doteq 128.22$), originating an

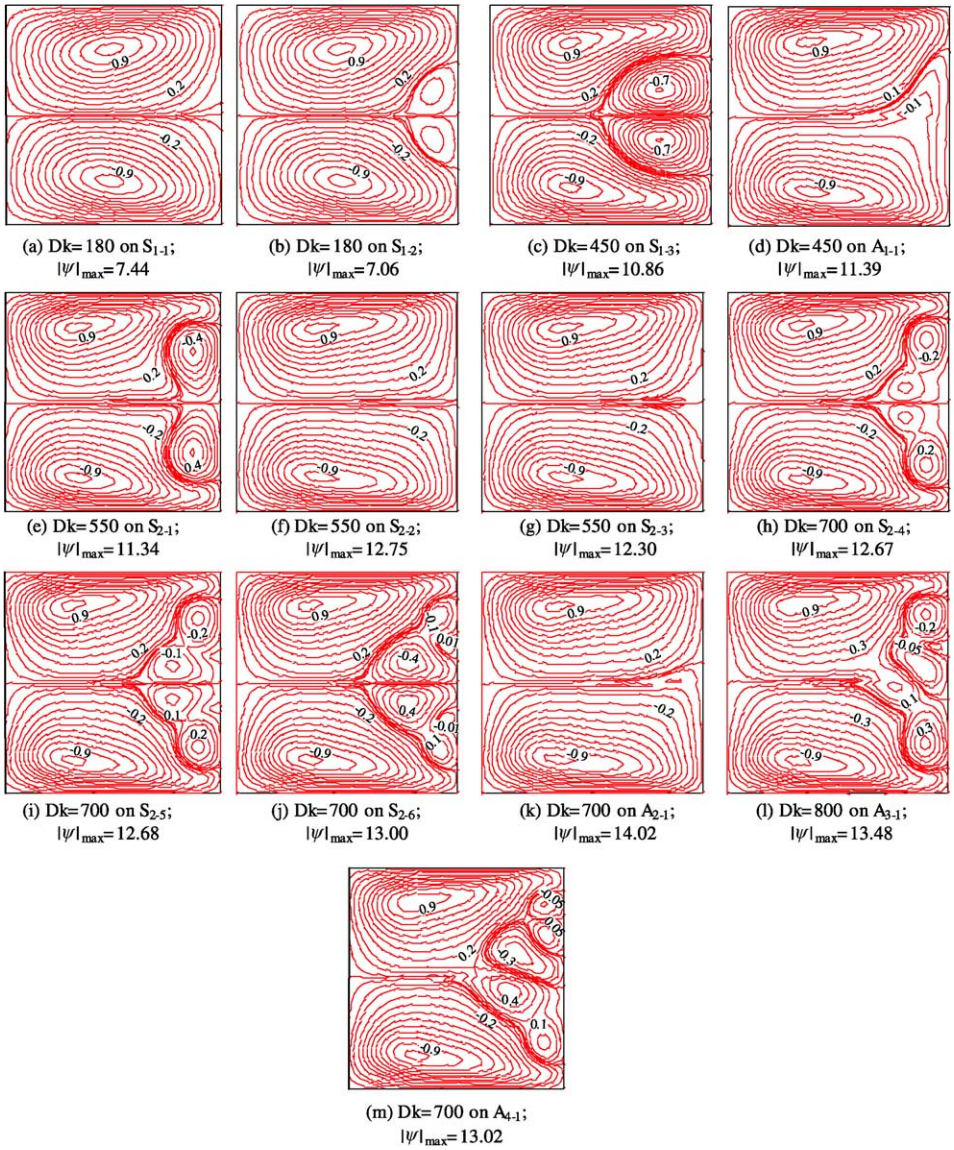

Fig. 3. Typical secondary flows on various solution sub-branches.

asymmetric solution branch A_1. A_1 has five limit points A_1^1–A_1^5. The limit point A_1^1 divides the branch into upper sub-branch $A_{1\text{-}1}$ and lower sub-branch $A_{1\text{-}2}$. The solutions on $A_{1\text{-}2}$ can be formed by mirror images of corresponding solutions on $A_{1\text{-}1}$ at the same Dk. While the sub-branch $A_{1\text{-}1}$ contributes, through the two limit points A_1^2 and A_1^3, three solutions for any value of Dk in a very small range $355.72 < Dk < 357.41$, the difference among these three solutions is negligibly small. Flows on $A_{1\text{-}1}$ are essentially an asymmetric two-cell state as shown in Fig. 3(d) for $Dk = 450$.

The solution branch S_2 is an isolated symmetric branch. It is divided into six sub-branches $S_{2\text{-}1}$–$S_{2\text{-}6}$ by five limit points S_2^1–S_2^5. To illustrate the flow structure and its evolution on each sub-branches, Fig. 3(e)–(j) show some typical secondary flow patterns of this branch at $Dk = 550$ and 700. The flow on $S_{2\text{-}1}$ is a four-cell state (Fig. 3(e)). However, this four-cell structure differs from the one on $S_{1\text{-}3}$ (Fig. 3(c)) mainly on the shape and size of Dean vortices. Two Dean vortices here stretch along span direction rather than the radial direction. The spanwise distance between centers of two Dean vortices is noticeably larger than that of the four-cell flow on $S_{1\text{-}3}$. The flow on $S_{2\text{-}2}$ is a two-cell state (Fig. 3(f)), which is qualitatively similar to that on $S_{1\text{-}1}$, but with a stronger secondary flow. The flow on $S_{2\text{-}3}$ is a

weak four-cell state with a pair of very weak Dean vortices (Fig. 3(g)).

The limit point S_2^3 leads the weakly four-cell flow on $S_{2\text{-}3}$ to a six-cell state on $S_{2\text{-}4}$ with two pairs of Dean vortices along the outer wall (Fig. 3(h)). The second pair appears because of the splitting of the original pair. It could be interesting to study, in the future, the relation between this vortex splitting and the one due to the Eckhaus instability [37]. The secondary flow on this sub-branch evolves to a stronger one through the growth of second pair of Dean vortices as Dk increases. Flows on $S_{2\text{-}5}$ and $S_{2\text{-}6}$ are a eight-cell state with three pairs of Dean vortices (Fig. 3(i) and (j)). The third pair is formed from the outer wall. This differs from the mechanism responsible for the appearance of the second pair. As usual, the secondary flows on $S_{2\text{-}5}$ and $S_{2\text{-}6}$ becomes stronger as Dk increases. For the same value of Dk, the eight-cell structure on $S_{2\text{-}6}$, the third pair of Dean vortices in particular, is stronger in strength than that on $S_{2\text{-}5}$.

In addition to the five limit points, the solution branch S_2 has also three symmetry-breaking bifurcation points B_2, B_3 and B_4, originating three asymmetric solution branches A_2, A_3 and A_4, respectively. Each of these branches has one limit point dividing the branch into a upper sub-branch ($A_{2\text{-}1}$, $A_{3\text{-}1}$ or $A_{4\text{-}1}$) and a lower sub-branch ($A_{2\text{-}2}$, $A_{3\text{-}2}$ or $A_{4\text{-}2}$). Solutions on the lower sub-branches are the mirror images of the corresponding solutions on the upper sub-branches at the same Dk. Fig. 3(k)–(m) detail secondary flow structures on these three branches. The flow on the $A_{2\text{-}1}$ is an asymmetric two-cell state (Fig. 3(k), qualitatively similar to that on $A_{1\text{-}1}$) while it is an asymmetric seven-cell structure on both $A_{3\text{-}1}$ and $A_{4\text{-}1}$ (Fig. 3(l) and (m)).

3.2. Stability of multiple solutions

Recognizing that there is no study on dynamic responses of multiple solutions to finite random disturbances in the literature, a relatively comprehensive transient computation is made to examine the dynamic behavior and stability of 56 typical steady solutions with respect to three sets of finite random disturbances with $d = 4\%$, 10%, and 15% respectively. Here d is the maximum percentage of disturbing value over the initial steady value. It is found that the final dynamic evolution after a short transient temporal period is independent of the initial disturbances for all solutions in the region $0 \leqslant Dk \leqslant 650$. The results presented in this paper are those obtained from the disturbance with $d = 10\%$ unless otherwise stated. At any fixed value of Dk in the range $0 \leqslant Dk \leqslant 620$, all steady solutions develop, after initial finite random disturbances, to the same final state. There is no co-existence of two or more stable states in this range within the scope of the present study. The stability of solutions on the sub-branch $S_{2\text{-}2}$ changes as Dk changes even without passing any bifurcation or limit point. In particular, the sub-branch is unstable in the range $310.71 \leqslant Dk \leqslant 375$, stable in the range $375 < Dk \leqslant 620$ and unstable again in the range $620 < Dk \leqslant 643.3$.

Five sub-ranges are identified with each having distinct dynamic responses to the finite random disturbances (Fig. 2). The first is from $Dk = 0$ to $Dk = 191.27$ (S_1^1), where the finite random disturbances lead all steady solutions at any fixed Dk to a two-cell steady state on $S_{1\text{-}1}$ with the same Dk. The second covers the range $191.27 < Dk \leqslant 375$ where all steady solutions evolve to a temporal periodic solution. In the third sub-range $375 < Dk \leqslant 620$, the finite random disturbances lead all solutions to a two-cell steady state on $S_{2\text{-}2}$ with the same Dk. The fourth sub-range ranges from $Dk = 620$ to $Dk = 650$ where the solutions response to the finite random disturbances in the form of temporal oscillation with intermittency, a forecasting signal of chaotic flows. In the last sub-range $Dk > 650$, any finite random disturbance will deviate the solutions to a chaotic oscillation.

3.2.1. $0 \leqslant Dk \leqslant 191.27$

Winters [19] found that the Jacobian determinant is negative on $S_{1\text{-}3}$ and the part of $S_{1\text{-}2}$ between B_1 and S_1^1, and positive on $S_{1\text{-}1}$ and the part of $S_{1\text{-}2}$ between S_1^2 and B_1. The conclusion drawn from Winters [19] is thus that the solutions on $S_{1\text{-}3}$ and the part of $S_{1\text{-}2}$ between B_1 and S_1^1 are unstable, but the solutions on $S_{1\text{-}1}$ and the part of $S_{1\text{-}2}$ between S_1^2 and B_1 *might* stable. Our linear stability analysis confirms his founding of the linear instability of $S_{1\text{-}3}$ and the part of $S_{1\text{-}2}$ between B_1 and S_1^1. Furthermore, our linear stability analysis, which is capable to ascertain the linear stability conclusively by finding all eigenvalues, shows that the solution on $S_{1\text{-}1}$ is linearly stable, but the solution on the part of $S_{1\text{-}2}$ between S_1^2 and B_1 is linearly unstable.

Fig. 4(a) typifies the responses of solutions on $S_{1\text{-}1}$ to the finite random disturbances. In the figure, the deviation of velocity components from their initial steady values is plotted against the time τ at (0.9, 0.14), (0.94, 0.1) and (0.96, 0.06) for $Dk = 180$. We plot both radial (u-) and spanwise (v-) velocity components for the first point (0.9, 0.14) while only u-velocity component is shown for the last two points. To facilitate the comparison, we use these four velocity components (either velocity itself or derivation velocity from its initial steady value) in all figures illustrating dynamic responses of multiple solutions to the finite random disturbances. It is observed that all deviation velocities vanish after a short period of time. The flows and temperature profiles return to their initial steady ones shown in Fig. 3(a). Therefore, the solutions on $S_{1\text{-}1}$ are also stable with respect to the finite random disturbances in addition to their linear stability.

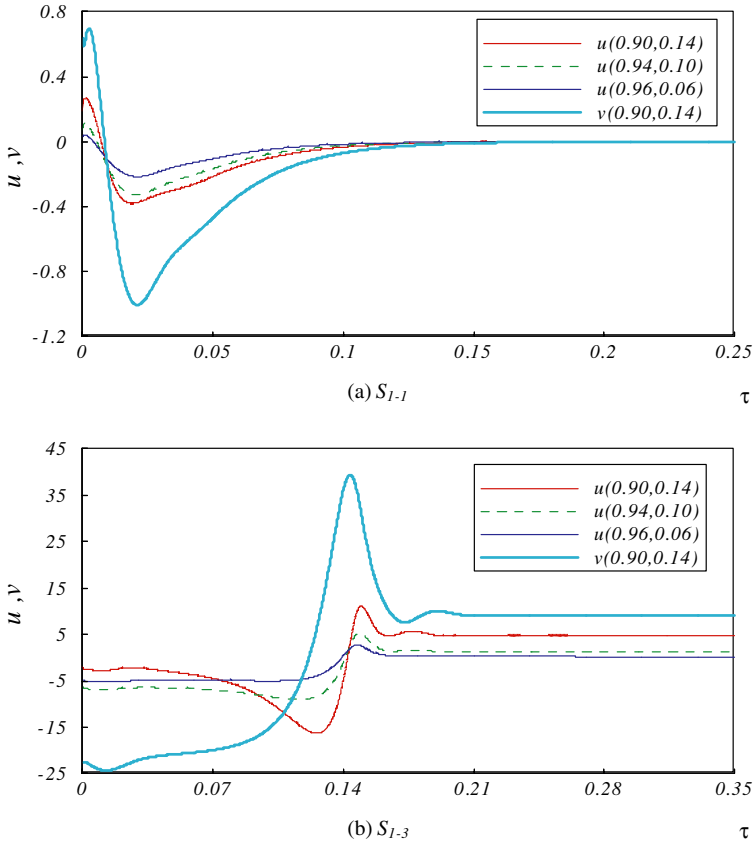

Fig. 4. Dynamic response of two solutions at $Dk = 180$ on $S_{1\text{-}1}$ and $S_{1\text{-}3}$, respectively, to finite random disturbances: evolution to stable steady two-cell state on $S_{1\text{-}1}$.

Fig. 4(b) illustrates the typical response of solutions on $S_{1\text{-}3}$ to the finite random disturbances. It shows that the finite random disturbances lead eventually the solutions on this unstable sub-branch to the stable one on $S_{1\text{-}1}$ at the same Dk. This is further be confirmed by our detailed check of flow and temperature fields and is also true for the solutions on $S_{1\text{-}2}$. Therefore, the solutions on $S_{1\text{-}2}$ and $S_{1\text{-}3}$ are unstable to the finite random disturbances and response the disturbances by evolving to the stable solution on $S_{1\text{-}1}$ at the same Dk.

3.2.2. $191.27 < Dk \leqslant 375$

Winters [19] found that the Jacobian determinant is positive on A_1. Therefore, the linear stability of this branch is not conclusive. Our linear stability analysis shows that this branch is linearly unstable. The linear stability of $S_{1\text{-}3}$ and $S_{2\text{-}1}$ examined in [19] is reconfirmed to be unstable in this range by our linear stability analysis. In contract to [19], however, we found that $S_{2\text{-}2}$ is linearly unstable in this range.

The dynamic response of the solution at $Dk = 300$ on $A_{1\text{-}1}$ is shown in Fig. 5(a). The finite random disturbances here lead the solution to a temporal periodic state with a period of 0.159. Some typical secondary flow patterns are detailed in Fig. 5(b) within one period of dimensionless time τ. We clearly observe the temporal oscillations between symmetric/asymmetric two-cell flows and symmetric/asymmetric four-cell flows, a phenomenon observed experimentally in [22,23,26,27]. A detailed study by the dynamic responses of solutions on other branches at $Dk = 300$ and the comparison of flow and temperature fields within one period show that the finite random disturbances lead all the solutions at the same Dk to the same periodic oscillation.

A similar dynamic evolution pattern exists for all cases with different values of Dk. This signals the similarity of flow and temperature fields within one period among the periodic states at different values of Dk in the range $191.27 < Dk \leqslant 375$. Our detailed examination of flow and temperature fields has confirmed this, and shown that the flow structures in Fig. 5(b) are typical for all Dk.

The variation of the period with Dk is shown in Fig. 5(c). It is observed that the period first increases with Dk,

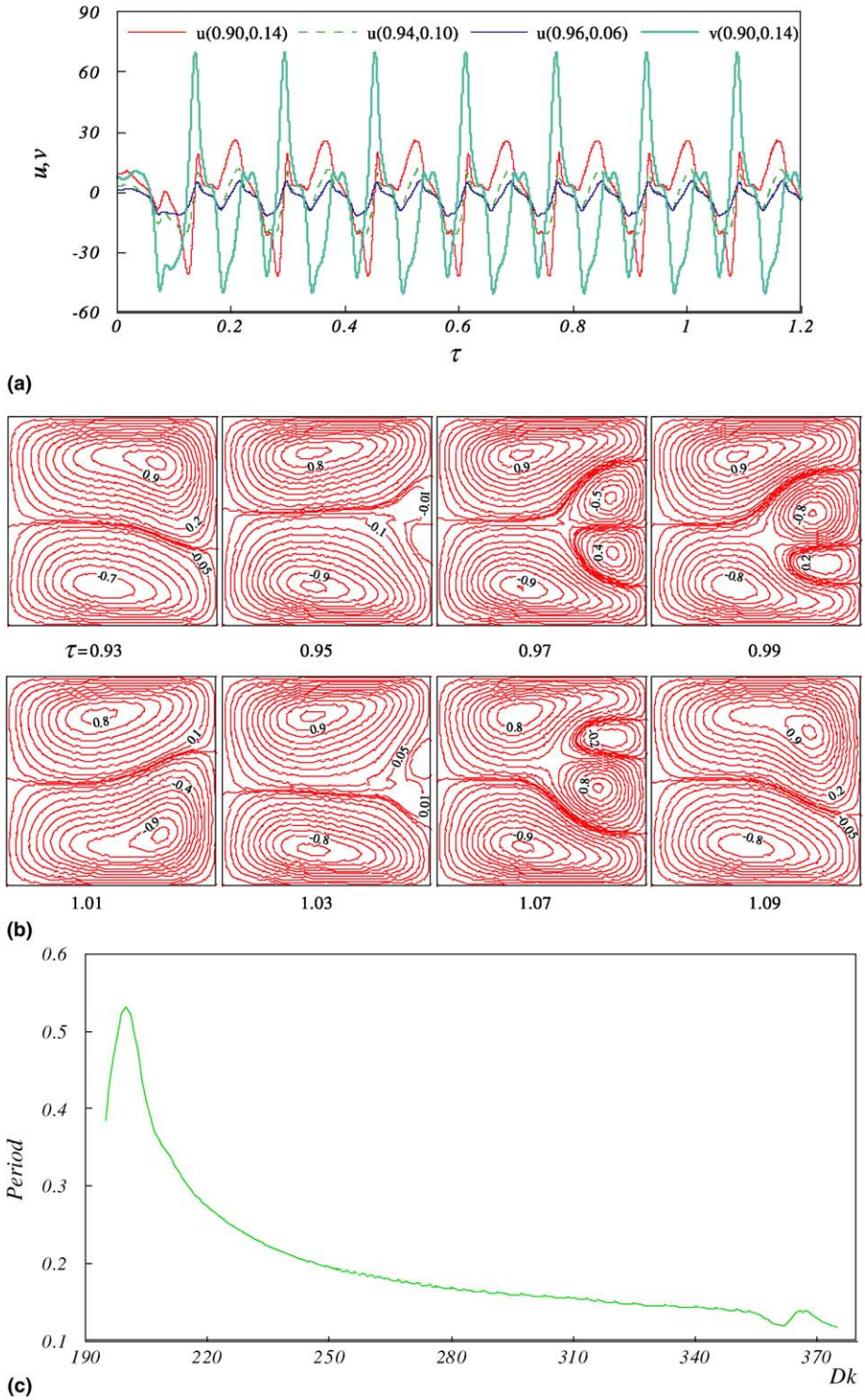

Fig. 5. Response to finite random disturbances in form of periodic oscillation in $191.23 < Dk \leqslant 375$. (a) Dynamic response of the solution at $Dk = 300$ on $A_{1\text{-}1}$ to finite random disturbances: periodic oscillation (period = 0.159). (b) Typical secondary flow patterns in one period of temporal periodic oscillation from the solution at $Dk = 300$ on $A_{1\text{-}1}$. (c) Variation of period with Dk.

and then decreases. But, it increases once again slightly around $Dk = 362$ and then decreases as Dk increases. There is no period-doubling bifurcation. Here, the temporal periodic oscillation serves as the transition from one stable steady flow in $0 \leqslant Dk \leqslant 191.27$ to another in $375 < Dk \leqslant 620$ as discussed in the next section.

The dynamic responses of solutions on A_1 in this range tend to show that B_1 is a sub-critical Hopf bifurcation point.

3.2.3. $375 < Dk \leqslant 620$

In this range, our linear stability analysis shows that $S_{2\text{-}1}$ is linearly unstable, but $S_{2\text{-}2}$ is linearly stable. It is of special interest that the linear stability of $S_{2\text{-}2}$ changes from unstable in the last range to stable in this range. Daskopoulos and Lenhoff [20] found that $S_{2\text{-}4}$ is linearly stable to symmetric disturbances. However, our linear stability analysis shows that it is linearly unstable to the asymmetric disturbances.

The two-cell state on $S_{2\text{-}2}$ is not only linearly stable but also stable to the finite random disturbances in this sub-range. This can be referred by the typical response of the solution at $Dk = 610$ on this sub-branch to the disturbances in Fig. 6(a). Another striking feature can be obtained by comparing the dynamic process in Fig. 6(a) with that in Fig. 4. The transient solutions approach their stable steady states asymptotically for $S_{1\text{-}1}$, but in oscillation for $S_{2\text{-}2}$. The oscillation in Fig. 6(a) may be reviewed as the over-damped oscillation with the damping effect being weaker at higher Dk, and thus a longer oscillating time. This difference is in agreement with findings of our linear stability analysis: the eigenvalues with maximum real part are real-valued for $S_{1\text{-}1}$, but complex-valued for $S_{2\text{-}2}$.

In this sub-range of the parameter space, the finite random disturbances will lead all the other solutions to the two-cell steady state on $S_{2\text{-}2}$ at the same Dk. Fig. 6(b) typifies this process by the dynamic response of the solution at $Dk = 550$ on $S_{2\text{-}1}$ to the disturbances.

3.2.4. $620 < Dk \leqslant 650$

In this sub-range, all solution branches are linearly unstable. The $S_{2\text{-}2}$, in particular, loses its linear stability gained in the last sub-range. While three sets of finite

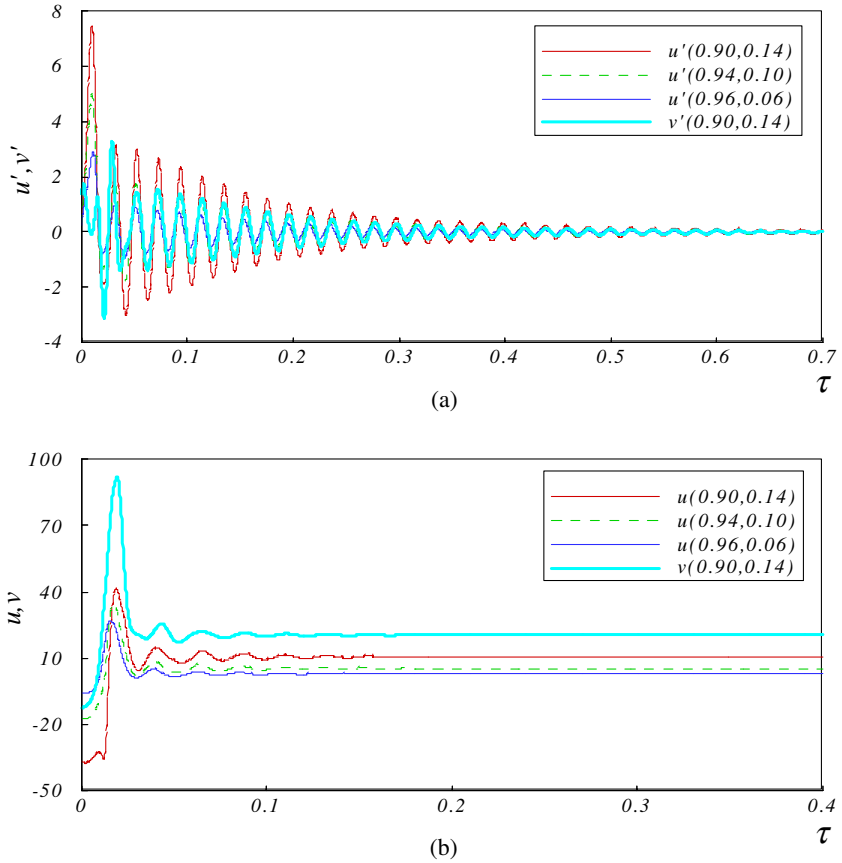

Fig. 6. Dynamic responses of solutions to finite random disturbances: evolution to stable steady two-cell state on $S_{2\text{-}2}$. (a) $Dk = 610$ on $S_{2\text{-}2}$, (b) $Dk = 550$ on $S_{2\text{-}1}$.

random disturbances lead each solution to the same final temporal oscillation state, the solutions at different solution branches at the same Dk respond the disturbances differently in the sense that the final oscillation is different. However, for a fixed value of Dk, all the oscillation are around the steady solutions on $S_{2\text{-}2}$ before $Dk = 643.30$ (point S_2^2) and around the steady solutions on A_2 after $Dk = 643.30$. Whether $A_{2\text{-}1}$ or $A_{2\text{-}2}$ is difficult to distinguish because they are very close. Therefore, $S_{2\text{-}2}$ and A_2 differ from the other solution branches in this aspect.

Fig. 7 details the dynamic responses to the disturbances of the solutions at $Dk = 630$ on $S_{2\text{-}1}$ (Fig. 7(a)), and at $Dk = 638$ on $S_{2\text{-}2}$ (Fig. 7(b)), respectively. It is observed that there exists intermittent aperiodic bursts in the oscillation, one of routes to chaos [29,38,39]. The oscillation is quasi-periodic between two bursts with the periodicity being degraded as Dk increases. The appearance frequency of bursts increases as Dk increases.

Fig. 8 details the secondary flow during quasi-periodic oscillations (Fig. 8(a), (e), (f)) and bursts (Fig. 8(b)–(d)) for the case shown in Fig. 7(a). It is observed that the flow oscillates among symmetric/asymmetric two-cell patterns during quasi-periodic oscillations but among symmetric/asymmetric four-cell structures during bursts.

3.2.5. $650 < Dk \leqslant 800$

In this sub-range, all solution branches are also linearly unstable. Fig. 9(a) shows the dynamic response of the solution at $Dk = 800$ on $A_{3\text{-}1}$ to the finite random disturbance with $d = 10\%$. The bursts are still observed, but, with a high appearance frequency and a generally small amplitude. The oscillation between two bursts, however, cannot be reviewed as quasi-periodic any more. The power spectra of four velocity temporal series in Fig. 9(a) are constructed by the Fourier transformation and shown in Fig. 9(b). They contain the broadband noise, indicating the flow being chaotic [29]. The sensitivity to the initial conditions serves as another criterion of chaos [40]. Fig. 9(c) shows the dynamic response of the solution to the disturbance with $d = 15\%$. The oscillation in Fig. 9(c) is observed to be different with that in Fig. 9(a). This further confirms that the oscillation in Fig. 9(a) is chaotic. Fig. 9(d) details some typical secondary flow patterns for the temporal chaotic flow shown in Fig. 9(a). It is observed that the flow oscillates among four-cell patterns during bursts ((iii) and (iv) in Fig. 9(d)) but among two-cell and three-cell

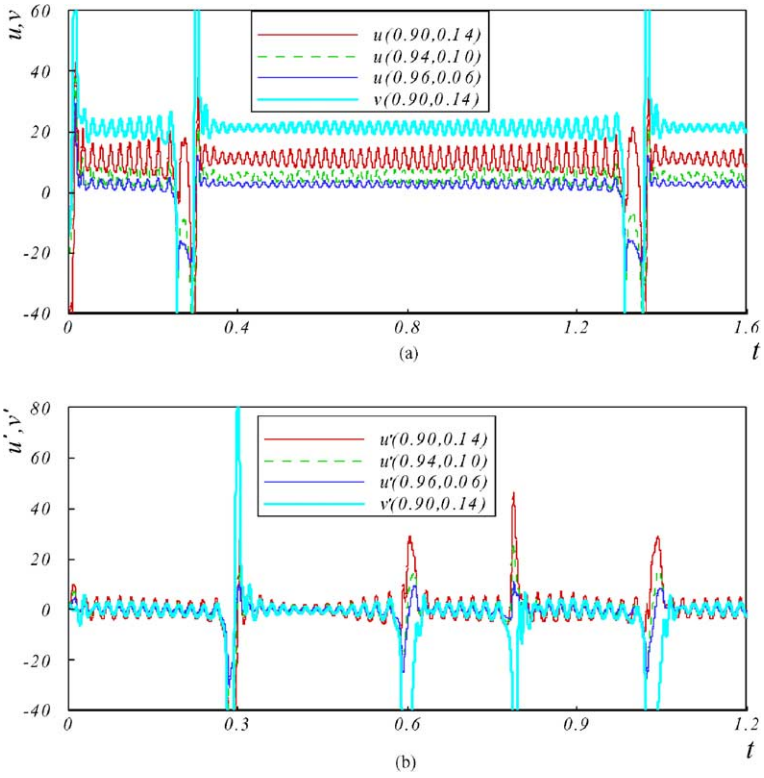

Fig. 7. Dynamic responses of solutions to finite random disturbances: intermittency. (a) $Dk = 630$ on $S_{2\text{-}1}$, (b) $Dk = 638$ on $S_{2\text{-}2}$.

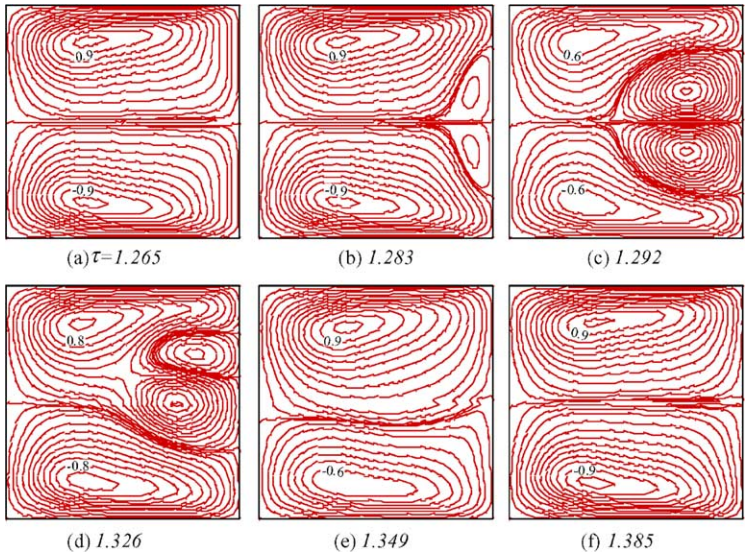

Fig. 8. Typical secondary flow patterns of intermittent flow from solution at $Dk = 630$ on $S_{2\text{-}1}$.

structures during the other period ((i) and (ii) in Fig. 9(d)).

In spite of their chaotic feature, all oscillations from different solution branches and different disturbances at the same Dk appear around a common equilibrium state, the steady solution on A_2. As $A_{2\text{-}1}$ and $A_{2\text{-}2}$ are very close, it is difficult to distinguish whether it is $A_{2\text{-}1}$ or $A_{2\text{-}2}$. Fig. 10 shows dynamic responses of three solutions at $Dk = 700$ on different solution branches to the disturbances. It is observed that all u's evolve into A_2 at $Dk = 700$ in a short time period and then oscillate chaotically around it. This has also been confirmed by our detail check of flow patterns and temperature profiles. Therefore, the solution branch A_2 differs from the others in its stability.

The transition from the intermittent oscillation to the chaotic oscillation is believed to be a smooth process characterized by the increase of appearance frequency and the decrease of the amplitude of bursts as the increase of Dk. As the solution at $Dk = 660$ on $A_{4\text{-}1}$ responses to the disturbance also in the form of chaotic oscillation, it is not unreasonable to conjecture that the transition takes place gradually within $Dk = 650$–660.

4. Concluding remarks

The governing differential equations from the conservation laws are discretized by the finite volume method to obtain discretization equations. The discretization equations are solved for parameter-dependence of flow and temperature fields by the Euler–Newton continuation with the solution branches parameterized by the pseudo-Dean number Dk, the arc-length or the local variable. The bifurcation points are detected by the test function. The Hopf bifurcation point is determined by the transient computation. The branch switching is made by a scheme approximating the difference between branches proposed in [29]. Two symmetric and four asymmetric solution branches are found. Among them, three new asymmetric branches are with either two-cell or seven-cell flow structure. They arise from three new symmetry-breaking bifurcation points on the symmetric branch S_2. The bifurcation point B_1 is found to be a subcritical Hopf point.

The linear stability of multiple solutions is made by solving the eigenvalue system for all eigenvalues. This can lead to a conclusive result regarding the linear stability of solutions. $S_{1\text{-}1}$ ($0 \leqslant Dk \leqslant 191.27$) and the part of $S_{2\text{-}2}$ between $Dk = 375$ and $Dk = 620$ are linearly stable. Both are with a two-cell flow structure. All the other sub-branches and branches are linearly unstable. In particular, $S_{2\text{-}4}$ is linearly unstable to the asymmetric disturbances although it is stable to the symmetric disturbances. $S_{2\text{-}2}$ can gain and lose its linear stability without passing any bifurcation or limit points as Dk changes.

The dynamic responses of multiple solutions to the 2D finite random disturbances are examined by the direct transient computation. The solutions are found to respond three sets of finite random disturbances in the same manner in the range with $Dk \leqslant 650$. At any fixed value of Dk in the range $0 \leqslant Dk \leqslant 620$, all steady solutions develop, after the initial finite random disturbances, to the same final state. The finite random disturbances are found to lead the steady solutions to a

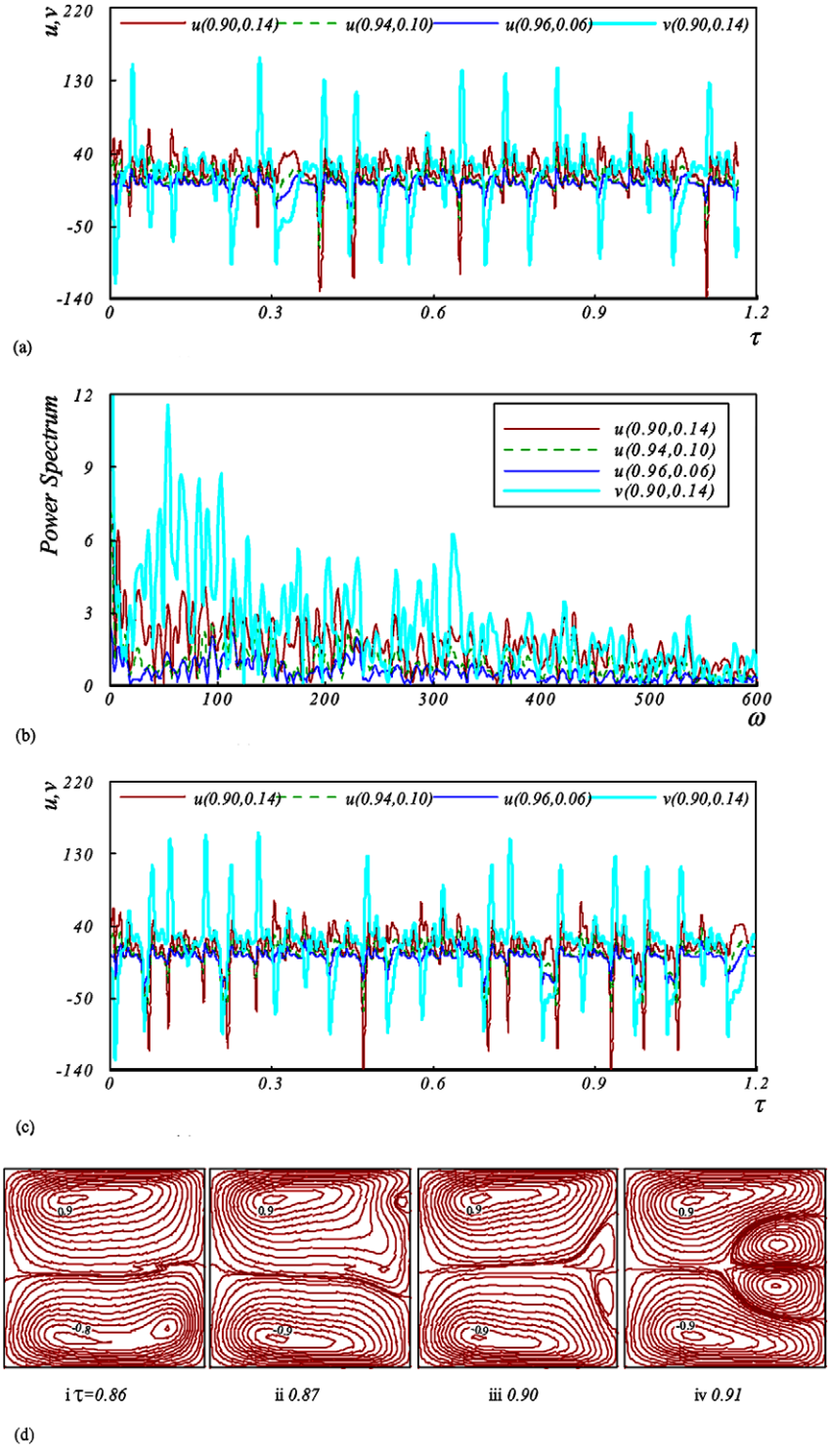

Fig. 9. Dynamic response of the solution at $Dk = 800$ on $A_{3\text{-}1}$ to finite random disturbances: chaotic oscillation. (a) Dynamic response to the finite random disturbance with $d = 10\%$. (b) Power spectrum of the chaotic oscillation in (a). (c) Dynamic response to the finite random disturbance with $d = 15\%$. (d) Typical secondary flow patterns of chaotic flow from the solution at $Dk = 800$ on $A_{3\text{-}1}$.

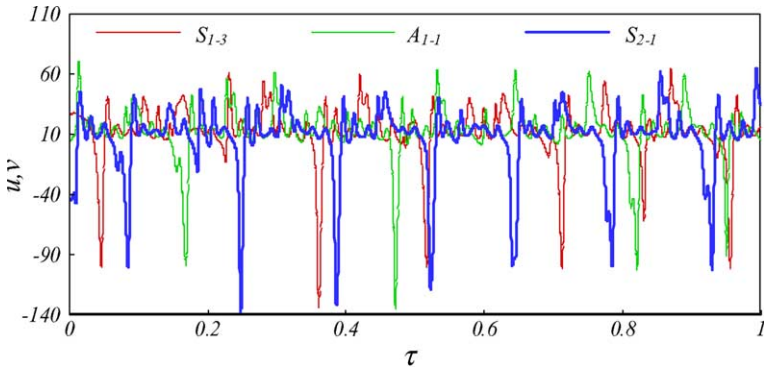

Fig. 10. Dynamic responses of u at (0.9, 0.14) to finite random disturbances for three solutions at $Dk = 700$.

stable steady two-cell state on $S_{1\text{-}1}$ in $0 \leqslant Dk \leqslant 191.27$, a temporal periodic oscillation between symmetric/asymmetric two-cell flows and symmetric/asymmetric four-cell flows in $191.27 < Dk \leqslant 375$, another stable steady two-cell state on $S_{2\text{-}2}$ in $375 < Dk \leqslant 620$, an intermittent oscillation in $620 < Dk \leqslant 650$, and a chaotic oscillation in $650 < Dk \leqslant 800$. The intermittent flow is characterized by the flow oscillation among the symmetric/asymmetric two-cell patterns during the period between two bursts and among the symmetric/asymmetric four-cell structures during the burst. The chaotic flow is, on the other hand, featured by the flow oscillation among the four-cell patterns during the burst, and the two-cell and three-cell structures during the other period.

Acknowledgements

Authors are indebted to Professor R. Seydel for his suggestion and discussion on numerical methods. LW wishes to thank Professors K.C. Cheng, K. Nandakumar, W.H. Finlay and J.H. Masliyah for their valuable discussion over years. The financial support from the Research Grants Council of Hong Kong (RGC), the CRCG, and the Outstanding Young Researcher Award of the University of Hong Kong to LW is gratefully acknowledged.

References

[1] W.R. Dean, Fluid motion in a curved channel, Proc. Roy. Soc. A 121 (1928) 402–420.
[2] S.A. Berger, L. Talbot, L.-S. Yao, Flow in curved pipes, Ann. Rev. Fluid Mech. 15 (1983) 461–512.
[3] K. Nandakumar, J.H. Masliyah, Swirling flow and heat transfer in coiled and twisted pipes, Adv. Transp. Process. 4 (1986) 49–112.
[4] H. Itō, Flow in curved pipes, JSME Int. J. 30 (1987) 543–552.
[5] S.A. Berger, Flow and heat transfer in curved pipes and tubes, AIAA 91-0030 (1991) 1–19.
[6] H. Itō, Theory on laminar flow through curved pipes of elliptic and rectangular cross-sections, Rep. Inst. High Speed Mech. 1 (1951) 1–16.
[7] H.G. Cuming, The secondary flow in curved pipes, Aeronaut. Res. Counc. Rep. Mem. 2880 (1952).
[8] J.T. Stuart, Hydrodynamic stability, in: L. Rosenhead (Ed.), Laminar Boundary Layers, Oxford University Press, 1963, p. 505.
[9] K.C. Cheng, R.C. Lin, J.W. Ou, Fully developed laminar flow in curved rectangular channels, J. Fluids Eng. 98 (1976) 41–48.
[10] K.C. Cheng, M. Akiyama, Laminar forced convection heat transfer in curved rectangular channels, Int. J. Heat Mass Transfer 13 (1970) 471–490.
[11] K.C. Cheng, R.C. Lin, J.W. Ou, Graetz problem in curved square channels, J. Heat Transfer 97 (1975) 244–248.
[12] B. Joseph, E.P. Smith, R.J. Adler, Numerical treatment of laminar flow in helically coiled tubes of square cross section, AIChE J. 21 (1975) 965–974.
[13] K.C. Cheng, J. Nakayama, M. Akiyama, Effect of finite and infinite aspect ratios on flow patterns in curved rectangular channels, in: Flow Visualization, Hemisphere, 1979, pp. 181–186.
[14] S. Sugiyama, T. Hayashi, K. Yamazaki, Flow characteristics in the curved rectangular channels (visualization of secondary flow), Bull. JSME 26 (1983) 964–969.
[15] M. Akiyama, Laminar forced convection heat transfer in curved rectangular channels, M.Sc. thesis, Mechanical Engineering Department, University of Alberta, 1969.
[16] J.H. Masliyah, On laminar flow in curved semicircular ducts, J. Fluid Mech. 99 (1980) 469–479.
[17] K.H. Winters, R.C.G. Brindley, Multiple solutions for laminar flow in helically-coiled tubes, AERE Rep. 11373, AERE Harwell, UK, 1984.
[18] W. Shanthini, K. Nandakumar, Bifurcation phenomena of generalized Newtonian fluids in curved rectangular ducts, J. Non-Newtonian Fluid Mech. 22 (1986) 35–60.
[19] K.H. Winters, A bifurcation study of laminar flow in a curved tube of rectangular cross-section, J. Fluid Mech. 180 (1987) 342–369.
[20] P. Daskopoulos, A.M. Lenhoff, Flow in curved ducts: bifurcation structure for stationary ducts, J. Fluid Mech. 203 (1989) 125–148.

[21] B. Bara, K. Nandakuma, J.H. Masliyah, An experimental and numerical study of the Dean problem: flow development towards two-dimensional multiple solutions, J. Fluid Mech. 244 (1992) 339–376.
[22] K.C. Cheng, L.Q. Wang, The effects of centrifugal and Coriolis forces on secondary flow phenomena in rotating curved square channels: visualization for positive and negative rotations, Experimental and Numerical Flow Visualization, FED-172, ASME, 1993, pp. 359–367.
[23] K.C. Cheng, L.Q. Wang, Visualization of secondary flow phenomena in rotating curved square channels with positive and negative rotations, in: Proceedings of Fourth Triennial International Symposium on Fluid Control, Fluid Measurement, Fluid Mechanics, Visualization and Fluids, vol. 1, 1994, pp. 561–569.
[24] P.A.J. Mees, K. Nandakumar, J.H. Masliyah, Secondary instability of flow in a curved duct of square-cross section, J. Fluid Mech. 323 (1996) 387–409.
[25] P.A.J. Mees, K. Nandakumar, J.H. Masliyah, Steady spatial oscillations in a curved duct of square cross-section, Phys. Fluids 8 (1996) 3264–3270.
[26] L.Q. Wang, K.C. Cheng, Visualization of flows in curved channels with a moderate or high rotation speed, Int. J. Rotat. Mach. 3 (1997) 215–231.
[27] L.Q. Wang, K.C. Cheng, Visualization of flows in channels with curvature and rotation, in: L.L. Regel, W.R. Wilcox (Eds.), Centrifugal Processing, Kluwer Academic/Plenum Publishers, New York, 2001, pp. 339–360.
[28] S.R. Sankar, K. Nandakumar, J.H. Masliyah, Oscillatory flows in coiled square ducts, Phys. Fluids 31 (1988) 1348–1358.
[29] R. Seydel, Practical Bifurcation and Stability Analysis: From Equilibrium to Chaos, Springer-Verlag, New York, 1994.
[30] H. Miyazaki, Combined free and forced convective heat transfer and fluid flow in a rotating curved rectangular tubes, J. Heat Transfer 95 (1973) 64–71.
[31] L.Q. Wang, K.C. Cheng, Flow transitions and combined free and forced convective heat transfer in rotating curved channels: the case of positive rotation, Phys. Fluids 6 (1996) 1553–1573.
[32] R.K. Shah, A.L. Londong, Laminar Flow Forced Convection in Ducts, Academic, New York, 1978.
[33] S.W. Hong, S.M. Morcos, A.E. Bergles, Analytical and experimental results for combined forced and free convection in horizontal tubes, in: Proceedings of the Fifth International Heat Transfer Conference 3, 1974, pp. 154–158.
[34] T.L. Yang, Multiplicity and stability of flow and heat transfer in rotating curved ducts, Ph.D. thesis, Department of Mechanical Engineering, The University of Hong Kong, 2001.
[35] S.V. Patankar, Numerical Heat Transfer and Fluid Flow, Hemisphere Publishing Corporation, New York, 1980.
[36] L.Q. Wang, H.C. Wei, X.S. Zhou, Engineering Numerical Analysis, Shandong University Press, Jinan, 2002.
[37] Y. Guo, W.H. Finlay, Splitting, merging and wavelength selection of vortices in curved and/or rotating channel flow due to Eckhaus instability, J. Fluid Mech. 228 (1991) 661–691.
[38] Y. Pomeau, P. Manneville, Intermittent transition to turbulence in dissipative dynamical systems, Commun. Math. Phys. 74 (1980) 189–197.
[39] P. Bergè, P. Manneville, Y. Pomeau, Intermittency in Rayleigh–Benard convection, J. Phys. Lett. 41 (1980) L341–L345.
[40] H.O. Peitgen, H. Jürgens, D. Saupe, Chaos and Fractals, New Frontiers of Science, Springer-Verlag, New York, 1992.